Available online at www.sciencedirect.com
ScienceDirect
Ceramics International 36 (2010) 513–519
CERAMICS INTERNATIONAL
www.elsevier.com/locate/ceramint

Antibacterial properties, in vitro bioactivity and cell proliferation of titania–wollastonite composites

W. Ortega-Lara [a,*], D.A. Cortés-Hernández [a], S. Best [b], R. Brooks [c], A. Hernández-Ramírez [d]

[a] CINVESTAV IPN-Unidad Saltillo, Carr. Saltillo – Monterrey km 13, Apdo. Postal 663, C.P. 25000 Saltillo, Coahuila, México
[b] Department of Materials and Metallurgy, University of Cambridge, Pembroke Street, Cambridge CB2 3QZ, UK
[c] Orthopaedic Research Unit, Addenbrooks Hospital, Hills Road, Cambridge CB2 2QQ, UK
[d] Universidad Autónoma de Nuevo León, Fac. de Ciencias Químicas, Av. Universidad s/n, Cd. Universitaria, San Nicolás de los Garza, Nuevo León CP. 66400, Mexico

Received 15 July 2009; received in revised form 28 July 2009; accepted 6 September 2009
Available online 12 October 2009

Abstract

Titania–wollastonite materials that show high in vitro bioactivity, appropriate cell proliferation and antibacterial behavior have been developed. Titania–wollastonite compounds were synthesized by two different routes: (i) solid state reaction and (ii) sol–gel. The in vitro bioactivity assessment was performed by immersing samples in a simulated body fluid (SBF). The materials characterization, before and after immersion in SBF, was performed by SEM and EDS. Cytotoxicity was assessed by estimating cell proliferation and the antibacterial properties were evaluated by performing a kinetic study of a bacterium growth (*Burkhoderia cepacia*). In order to evaluate the band gap value UV–vis spectroscopy was performed. A faster apatite layer formation was observed on the samples processed by sol–gel. However, these agglomerates were smaller than those formed on the solid state reaction substrates. The highest inhibition of the bacteria growth and the highest cell proliferation were observed on the samples synthesized by solid state reaction.

Keywords: Wollastonite; Titania; Bioactivity; Cell proliferation; Antibacterial properties

1. Introduction

Since Hench's theory of bone-bonding ability was formulated, several bioactive compounds in the system SiO_2–CaO–Na_2O–P_2O_5 have been studied [1]. Bioglass 45S5 has demonstrated to be the highest bioactive glass, which bonds rapidly to bone, even to soft tissue [2,3]. Later, Kokubo and co-workers [4] reported that Na_2O–SiO–CaO glasses showed a higher strength besides bioactivity properties through the formation of a bonelike apatite layer when such materials were in contact with physiological fluids, even with acellular fluids (SBF). Therefore, for a material to bond to living bone, the material has to form a biologically active bonelike apatite layer on its surface when it is contact with SBF. Wollastonite has been recently studied as an implant material since it is bioactive, non-toxic and compatible with hard tissue. This apatite layer formed is dense, uniform and nucleates not only on flat surfaces, but also on curved surfaces, fibers, etc. [5]. $CaSiO_3$ and pseudowollastonite compounds were firstly investigated by De Aza and co-workers [6] as phosphorous-free materials that promote the formation of apatite in both, in vitro and in vivo tests. The synthesis method has an important effect on the performance of those compounds; wollastonite synthesized by sol–gel shows a faster apatite formation. According to various authors [7], the mechanism of apatite formation on materials rich in SiO–CaO begins with an ionic exchange between H_3O^+ ions, originally present in the SBF, and Ca ions from the substrate. Then, a silica layer is formed due the fact that the negative charged sites attract the H_3O^+ ions. The silanol layer formed attracts the solvated cations leading to the nucleation of the apatite layer. On other hand, in 1994 titania gel was found to be bioactive when exposed to SBF. Ceramic compounds based on titania and titanates generally show a higher elastic modulus and higher chemical durability than

* Corresponding author. Tel.: +52 844 4389600x9680; fax: +52 844 4389610.
E-mail addresses: dora.cortes@cinvestav.edu.mx, wlortega@yahoo.com (W. Ortega-Lara).

0272-8842/$36.00
doi:10.1016/j.ceramint.2009.09.024

Table 1
Processing methods and precursors used in the preparation of the wollastonite–titania materials.

	Synthesis method	TiO_2 precursor	$CaSiO_3$ precursor
Sample Type 1 (S1)	Solid state process	Rutile powder (wt. 50%)	Wollastonite powder
Sample Type 2 (S2)	Sol–gel method	Titanium butoxide	Calcium nitrate and TEOS
Sample Type 3 (S3)	Sol–gel method	Titanium butoxide	Wollastonite powder

silicates and phosphates. Similarly to compounds based in silicates, when titanium compounds are in contact with SBF, water molecules react with Ti–O–Ti bond to form additional Ti–OH groups. These groups induce apatite nucleation by increasing the ionic activity product of apatite in the fluid. Once the apatite has nucleated, apatite grows spontaneously by taking calcium and phosphate ions from the surrounding SBF [8–11]. Furthermore, titania has proved to posses photosensitivity properties, thus this material has applications in photovoltaic cells, total/partial degradation of pollutants, gas sensors and, as it shows appropriate physicochemical stability and mechanical integrity during the surgical process, titania is a highly potential material for bone replacement applications and, due to its photosensitivity properties, it may also be an ideal antibacterial material [12,13]. The photosensitivity phenomena is induced when a photon with enough energy promotes the jump of an electron from the basal level to an excited level (from the valence band to the conduction band), during this process the formation of a vacancy (hole) is involved. This created electron–hole pair recombines or form highly reactive species that are able to destroy surrounding species, such as bacteria nucleus, stopping the bacteria reproduction [14–17]. Titania/wollastonite composites have been prepared to improve pigments [18,19]. Recently, Ding and Liu [20–22] studied bioactivity and compatibility properties of non-heat-treated titania–wollastonite composites, the phases formed were only rutile and anatase (titania polymorphs) besides of wollastonite in a lamellar structure. After immersion in SBF, samples with higher content of wollastonite formed an apatite layer on the substrate. Furthermore, all composites demonstrated osteoblast proliferation resulting in cytocompatible materials.

The aim of this study is to develop bioactive, biocompatible and antibacterial materials from wollastonite and titania compounds obtained by sol–gel or solid state reaction followed by heat treatment. Different to that observed by Ding and Liu [20–22], the heat treatment of the samples of this work leads to the formation of other phases, such as titania, titanite, wollastonite and calcium titanate [23]. In this paper, the effect of the synthesis method on the antibacterial properties, the in vitro bioactivity and the cytocompatibility behavior was evaluated.

2. Materials and methods

As mentioned above, materials were synthesized by solid state reaction and sol–gel process. In this section the experimental procedure followed for the preparation of the materials by each method is presented.

2.1. Solid state reaction method, S1

The powder mixtures (Table 1) were ball-milled in polypropylene flasks with alumina balls using acetone as dispersing medium for 3 h. The slurries were dried at 80 °C for 24 h. The dried powders were then disk-shaped by uniaxial pressing at 150 MPa for 15 s. The disks were sintered at 1150 °C for 2 h.

2.2. Sol–gel methods, S2 and S3

Two different routes were used in order to obtain materials with a similar chemical composition to those obtained by solid state reaction. In the first one, the sol was prepared by mixing 0.39 mol of titanium butoxide (Aldrich, 97%+), 0.32 mol of tetraethyl-orthosilicate (TEOS) (Aldrich, 98%+) and 0.25 mol of calcium nitrate tetrahydrate (Aldrich, 99%+), the H_2O/TEOS molar ratio was 8 at pH 7. The mixture was vigorously stirred and heated at 60 °C for 1 h and dried at 80 °C for 48 h. The powder was heat treated at 400 °C for 2 h (S2, Table 1).

In the second sol–gel route, titanium butoxide was also used as the titania precursor, however, this reagent was directly mixed with wollastonite powder (S3, Table 1). The obtained powders were uniaxially pressed at 145 MPa for 20 s and heat treated at 500 °C for 2 h.

2.3. Immersion of samples in simulated body fluid (SBF)

The ceramic materials obtained were immersed in 100 ml of SBF under static conditions and kept at 36.5 °C for different periods of time (14 and 21 days). The SBF was prepared by dissolving appropriate amounts of reagent grade chemicals of sodium chloride (NaCl), sodium hydrogen carbonate ($NaHCO_3$), potassium chloride (KCl), dipotassium hydrogen phosphate ($K_2HPO_4{\cdot}3H_2O$), magnesium chloride hexahydrate ($MgCl_2{\cdot}6H_2O$), calcium chloride dihydrate ($CaCl_2{\cdot}2H_2O$) and sodium sulfate (Na_2SO_4) into de-ionized water and buffered to pH 7.4 at 36.5 °C with 1N hydrochloric acid or tris(hydroxymethyl) aminomethane ($((CH_2OH)_3CNH_2)$) [24]. After completing each immersion period, the samples were washed with de-ionized water and dried at room temperature.

The surface of the substrates, before and after immersion in SBF, was analyzed by scanning electron microscopy (SEM) (XL30 ESEM, Philips®), energy dispersive spectroscopy (EDS), X-ray diffraction (XRD) (X' Pert, Philips®) and phase-quantification was carried out with Sietronics XRD Trace Processing software, version 3.0.

The UV–vis absorption spectra of the solid samples were obtained by diffuse reflectance studies using a PerkinElmer

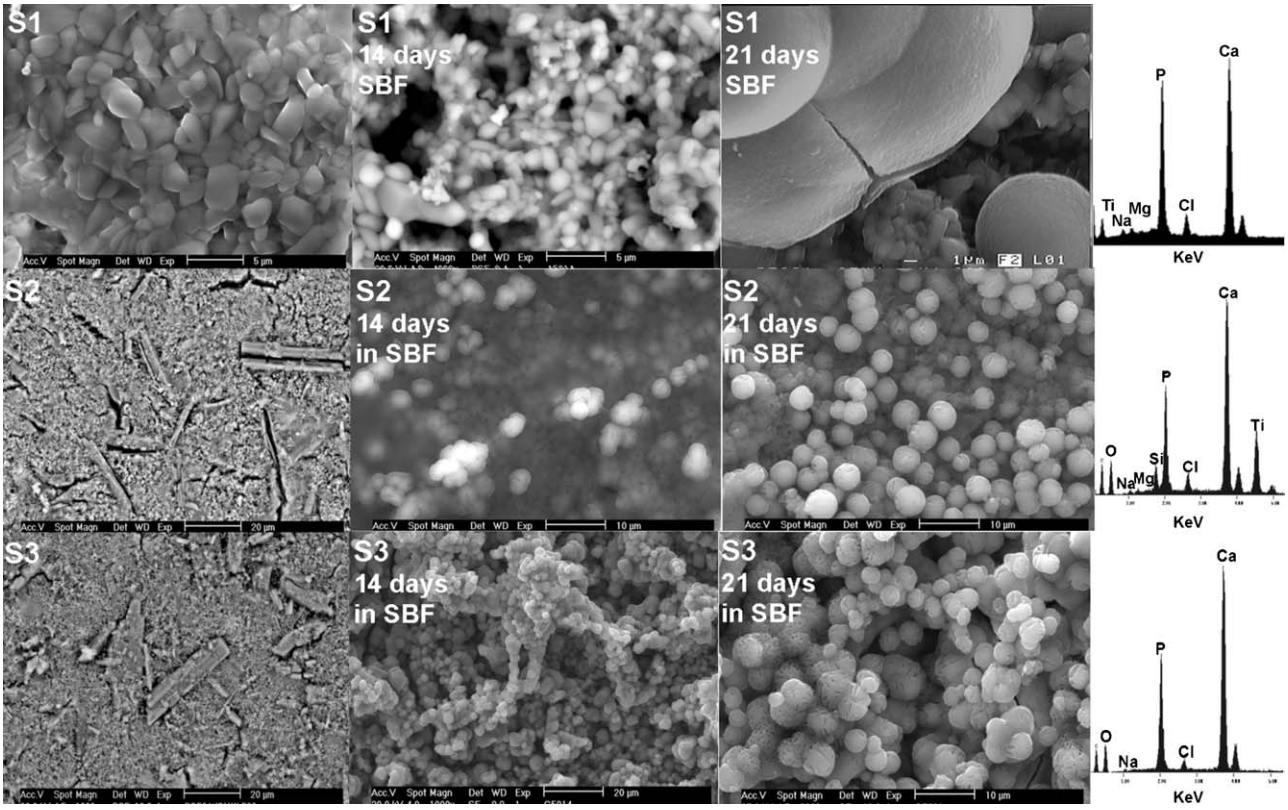

Fig. 1. SEM images of samples S1, S2 and S3 before and after 14 and 21 days of immersion in SBF and EDS spectra of the samples after 21 days of immersion.

spectrophotometer model Lambda 12 coupled to an integration Labsphere RSA-PE-20. A Spectralon standard USRS-99010 with 100% reflectance was used as reference.

2.4. Bacterial culture tests

For testing antibacterial properties *Burkholderia cepacia* was selected. This bacterium was cultivated in a nutrient broth containing dehydrated Bacto Nutrient Agar (DIFCO Lab). All glassware and test samples were sterilized in an autoclave at 121 °C and 15 atm for 15 min or by UV irradiation for 5 min before culturing. Each sterilized sample was immersed in 60 ml of nutrient broth containing 5 ml of inoculum. The flaks were covered and placed in a wrist-action shaker at 100 rpm (VWR Scientific, 1500E) and 36 °C. A sample of 5 ml of the solution was removed at different times and the bacteria proliferation was indirectly evaluated by turbidimetric readings (Spectrometer Spectronic 20D+ with a wavelength 600 nm, Milton Roy). The bacteria proliferation in the nutrient broth with no ceramic sample was used as a control.

2.5. Cell culture tests

For testing cytotoxicity a cell culture model (Alamar blue assays) was used. MG63 cells, originally isolated from human osteosarcoma cells, were cultured in a Dulbecco Modified Eagle's Medium (DMEM, Aldrich) containing penicillin/streptomycin (100 units/ml) and gentamicin (100 g/ml). Thirty microliters of 2×10^6 cells/ml were directly seeded on the substrates and on positive (a seeded polyethylene plate) and negative (non-seeded) controls and cultured for 1, 3, 5 or 7 days at 37 °C in a humidified air with 5% CO_2. After each period of time, Alamar blue (Serotech, Nalgene) was added to the cultured surface and kept for 3.5 h. The characterization was performed using a spectrophotometer (Fluorstar Optima, BMG, Labtech). The surface of samples after cell culturing was also analyzed by SEM.

3. Results and discussion

Fig. 1 shows SEM images and EDS spectra of the samples before and after immersion in SBF. The sample obtained by solid state reaction (before immersion in SBF, S1 in Fig. 1) shows a granular microstructure. In contrast, the morphology of the samples obtained by sol–gel consists of wollastonite whiskers embedded in a matrix composed of small particles (S2 in Fig. 1). The microstructure of the sample obtained also by sol–gel but by mixing titanium butoxide directly with wollastonite (S3 in Fig. 1) shows wollastonite whiskers of a larger size.

The XRD analysis reported in a previous work [23] is summarized in Table 2, which shows the phase quantification of substrates S1, S2 and S3. The main phases detected were rutile (JCPDS: 87-0920; 27.43°, 54.31°, 36.07°; tetragonal; TiO_2), wollastonite (JCPDS: 43-1460; 29.98°, 26.84°, 25.2°; Monoclinic; $CaSiO_3$-2 M) and a calcium silicon titanate, called titanite (JCPDS: 87-0256; 27.45°, 29.65°, 34.15° $CaTi(SiO_4)O$). Sample S3 presented only rutile and β-wollastonite due to the nature of the precursors used.

Table 2
Phase-quantification of S1, S2 and S3.

Sample	Phase-quantification			
	% TiO_2	% $CaSiTiO_4$	% β-$CaSiO_3$	$CaTiO_3$
S1	16.2	27.86	55.93	–
S2	21.58	38.26	22.95	18.19
S3	6.4	–	93.59	–

According to the XRD studies reported previously [23] a faster apatite formation was observed on the substrates synthesized by sol–gel than on those obtained by solid state reaction. These results are in agreement with the SEM and EDS analyses. The SEM images of the sample S1 after 14 days of immersion in SBF (Fig. 1) shows no a significant change in comparison with the sample before immersion. In contrast, the samples obtained by sol–gel (S2 and S3, Fig. 1) show the formation of a Ca, P-rich layer after 14 days of immersion. While the initial stages of the apatite nucleation can be observed on S1 after 21 days of immersion in SBF, a thicker and homogeneous apatite layer was formed on S2 and S3 after this period of time. The EDS spectra, which correspond to the samples after 21 days of immersion in SBF, show a high content of Ca and P. These results indicate that the samples obtained by sol–gel, especially S2, show a higher bioactivity than that observed on the sample obtained by solid state reaction (S1).

The UV–vis spectra are shown in Fig. 2, the band gap was evaluated by the following equation:

$$\alpha(h\nu) = A(h\nu - E_g)^{m/2} \quad (1)$$

in which, when $\alpha = 0$, the band gap value was $E_g = h\nu$. E_g was calculated from the UV–vis spectra by extrapolating a straight line from the absorption curve to the abscissa axis. The lowest E_g value corresponds to the sample processed by solid stated reaction followed by the samples synthesized by sol–gel S2 and S3. This behavior can be explained taking into account the Quantum Size Effect, which supposes that the particle size has a strong effect on the spectral properties of semiconductors when their size becomes comparable to the size of the exciton. Semiconductors such as CdS, ZnS and AgI have shown spectral blue shifts in the absorption band edge as a consequence of exciton confinement by decreasing the particle size. Several studies concerning the photophysics of TiO_2 colloids have reported this phenomenon [25]. The band gap of the material in a semiconductor is closely related with the formation of free

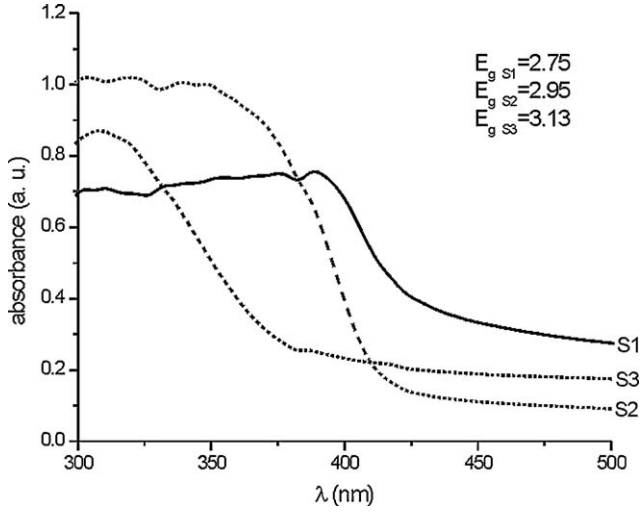

Fig. 2. UV–vis spectra of samples.

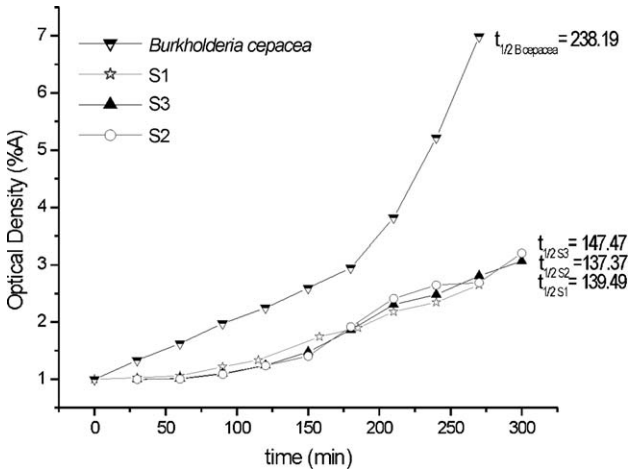

Fig. 3. Growth curves of *Burkhoderia cepacea* on wollastonite–titania samples at 37 °C in a nutrient broth.

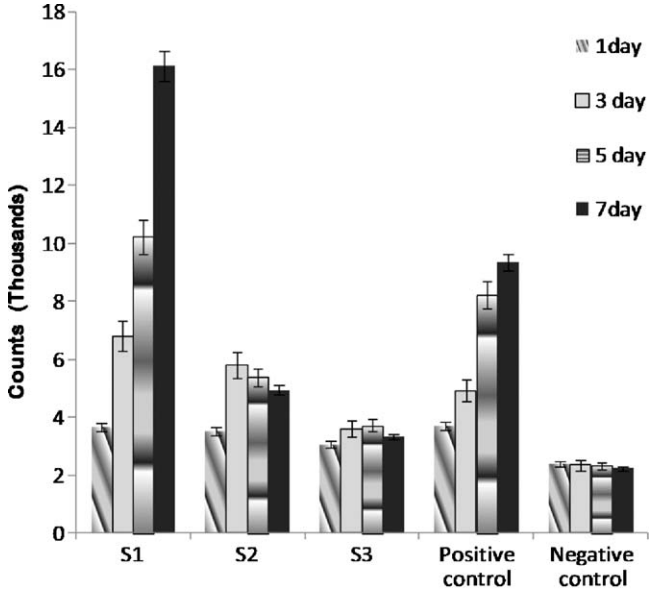

Fig. 4. Metabolic activity of cells on S1, S2, S3 and positive and negative controls.

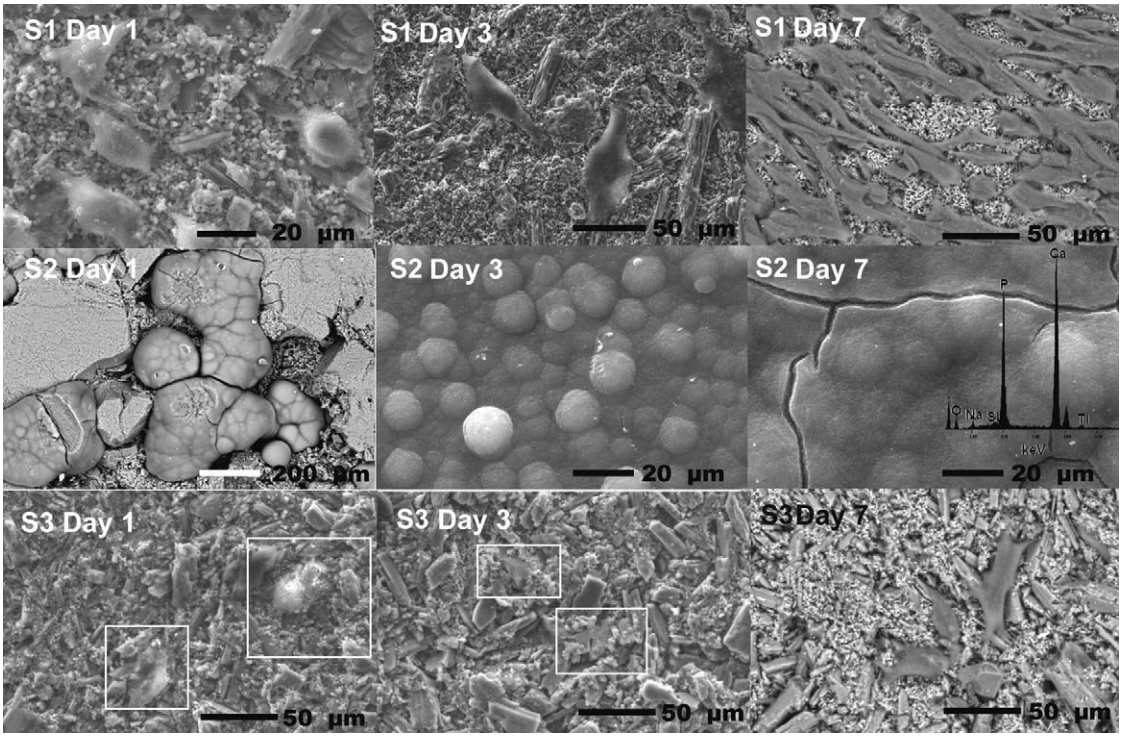

Fig. 5. SEM images of S1, S2 and S3 after 1, 3 and 7 days of cell culture testing.

radicals and unstable products which are responsible for the killing of bacteria [26].

Fig. 3 shows the kinetic study performed for analyzing the bacteria growth on S1, S2 and S3. As observed, the antibacterial behavior of these samples was similar. Nonetheless, the highest antibacterial activity was observed for S1 and S2, which showed lower E_g values than S3. The *B. cepacea* average time life decreases from 238.19 min in the nutrient broth (control) to 137.37 min for the sample S2 and 139.49 for the sample S1. There is no significant difference between the antibacterial activity of S1 and S2, considering the difference in particle size.

Fig. 4 shows the results of the cell culture assays. The cell activity on all the samples at days 1 and 3 is similar to that corresponding to the positive control and slightly higher than that of the negative control. An increase in cellular activity was observed on all the materials over the range between 1 and 3 days of culture. However, the cell activity on S2 and S3 stopped and decreased slightly at 5 and 7 days of culture. On the other hand, a substantial increase in cell proliferation with time was observed on sample S1. Furthermore, the cellular activity on this sample was considerably higher than that corresponding to the positive control over the 7 day culture period. It is important to remark that the surface of S1 was considerably smoother than that of S2 and S3. According to the literature [27,28], the effect of surface roughness is not totally understood due to several parameters, such as cell type, surface topography, physico-chemical properties, etc. Some works report that cell proliferation is linked to smooth surfaces [29,30], while others indicate that proliferation is related to roughness [31,32]. As the nature of the materials is very similar since their main compounds are wollastonite, TiO_2 and titanite, the results of this work indicate that human MG63 cells show a clear preference for smooth surfaces.

Fig. 5 shows SEM images of the cell cultured samples. A typical evolution of cells attachment with time (from 1 to 7 days) is observed. The image of S1 at day 1 shows some round cells that exhibit homogeneity in cytoplasmatic prolongation, larger cells are presented at day 3 showing lamellipodia, the

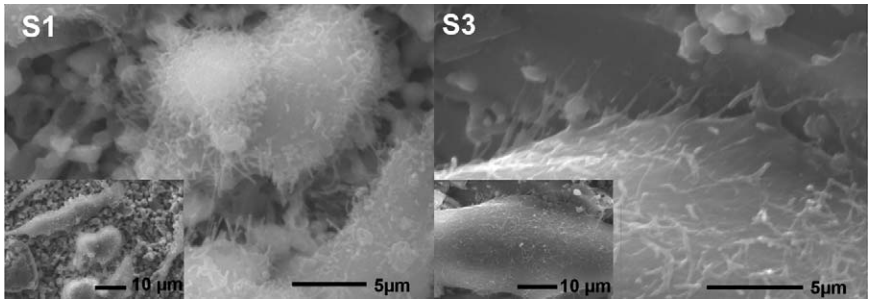

Fig. 6. SEM images (at high magnifications) of S1 and S3 after 7 days of cell culture testing.

apparition of these spindle cells may be associated to the proliferation increase as observed in Fig. 5. A higher cell proliferation is observed at day 7, a large amount of elongated cells are attached to the substrate and joined one to another by filopodia. In contrast, on sample S2, a crystalline Ca, P-rich compound was formed over the period culture with MG63 cells in nutrient broth (DMEM) and no cell attachment was observed. The formation of this compound may limit the cell growth, since it may be in competition with cells by nutrients. Although sample S3 shows a lower cell proliferation than S2 (Fig. 4), a localized area with round cells at day 1 can be observed in Fig. 6. These cells proliferated as a function of culture time and became spread; in this case, cells show a heterogeneous cytoplasmatic growth. Cells are better spread and flattened on S1 in contrast to those on selected areas of S3, a higher proliferation was also observed. It is well known that in the cell adhesion process are involved phenomena such as protein adsorption, contact of round cells to the substrate, attachment of those cells to the substrate and the cell spreading.

Fig. 6 shows SEM images of S1 and S3 after 7 days of culture. Spindle cells are attached to the surface of S1 by filopodia and microvilli and covered with ruffles. The image corresponding to S3 shows a spindle cell covered with microvilli anchorage to the substrate and covered with ruffles and some bundles. These images show also a comfortable growth.

4. Conclusions

Potentially bioactive wollastonite and titania-containing materials, which have also an appropriate antibacterial behaviour, can be obtained by either solid state reaction or sol–gel method. A thicker apatite layer was formed on the samples processed by sol–gel. However, as the sample processed by solid state reaction showed a smoother surface, a higher cell proliferation was observed by using this method. This may indicate that cell proliferation is closely related to smooth surfaces. The feasibility to obtain materials with similar band gap values (E_g) by both synthesis methods was demonstrated. Due to this similarity in band gap values, a high and similar antibacterial efficiency was observed in all the cases.

References

[1] L.L. Hench, R.J. Splinter, W.C. Allen, T.K. Greenlee, Bonding mechanisms at the interface of ceramic prosthetic materials, Journal of Biomedical Materials Research Symposium 2 (1971) 117–141.

[2] L.L. Hench, Bioceramics, Journal of the American Ceramic Society 81 (1998) 1705–1728.

[3] L.L. Hench, D.E. Clark, Physical chemistry of glass surfaces, Journal of Non-Crystalline Solids 28 (1978) 83–105.

[4] H.M. Kim, F. Miyaji, T. Kokubo, Bioactivity of Na_2O–CaO–SiO_2 glasses, Journal of the American Ceramic Society 78 (1995) 2405–2411.

[5] K. Hata, T. Kokubo, T. Nakamura, T. Yamamuro, Growth of a bonelike apatite layer on a substrate by a biomimetic process, Journal of the American Ceramic Society 78 (4) (1995) 1049–1053.

[6] P.N. De Aza, F. Guitián, S. De Aza, Bioeutectic: a new ceramic material for human bone replacement, Biomaterials 18 (1997) 1285–1291.

[7] M.I. Alemany, M.A. Velazquez de la Casa-Lillo, P.N. De Aza, Effect of materials processing methods on the in vitro bioactivity of wollastonite glass-ceramic materials, Journal of Non-Crystalline Solids 351 (2005) 1716–1726.

[8] P. Li, C. Ohtsuki, T. Kokubo, K. Nakanishi, N. Soga, K. de Groot, The role of hydrated silica, titania and alumina in inducing apatite on implants, Journal of Biomedical Materials Research 28 (1994) 7–15.

[9] T Kokubo, H.M. Kim, M. Kawashita, Novel bioactive materials with different mechanical properties, Biomaterials 24 (2003) 2161–2175.

[10] T. Kokubo, T. Matsushita, H. Takadama, Titania-based bioactive materials, Journal of the European Ceramic Society 27 (2007) 1553–1558.

[11] T. Kasuga, H. Kondo, M. Nogami, Apatite formation on TiO_2 in simulated body fluid, Journal of Crystalline Growth 235 (2002) 235–240.

[12] O. Carp, C.L. Huisman, A. Reller, Photoinduced reactivity of titanium dioxide, Progress in Solid State Chemistry 32 (2004) 33–177.

[13] N. Serpone, Is the band gap of pristine TiO2 narrowed by anion- and cation-doping of titanium dioxide in second-generation of photocatalyst? Journal of Physical Chemistry B 110 (2006) 24287–24293.

[14] A.K. Benabbou, Z. Derriche, C. Felix, P. Lejeune, C. Guillard, Photocatalytic inactivation of Escherichia coli. Effect of concentration of TiO_2 and microorganism, nature and intensity of UV irradiation, Applied Catalysis B: Environmental 76 (2007) 257–263.

[15] B Kim, D. Kim, D. Cho, S. Cho, Bactericidal effect of TiO_2 photocatalyst on selected food-borne phatogenic bacteria, Chemosphere 52 (2003) 277–281.

[16] K.P. Kühn, I.F. Chaberny, K. Massholder, M. Stickler, V.W. Benkz, H.G. Sonntag, L. Erdinger, Disinfection of surfaces by photocatalytic oxidation with titanium dioxide and UVA light, Chemosphere 53 (2003) 71–77.

[17] K.J. Shieh, M. Li, Y.H. Lee, S.D. Sheu, Y.T. Liu, Y.C. Wang, Antibacterial performance of photocatalyst thin film fabricated by defection effect in visible light, Nanomedicine: Nanotechnology, Biology and Medicine 2 (2006) 121–126.

[18] J.Z. Zhao, Z.C. Wang, L.W. Wang, H. Yang, M.Y. Zhao, The synthesis and characterization of TiO_2/wollastonite composite, Materials Letters 37 (1998) 149–155.

[19] J.Z. Zhao, Z.C. Wang, L.W. Wang, H. Yang, M.Y. Zhao, Differences between two TiO_2/wollastonite composites with wollastonite having different particle sizes, Materials Letters 41 (1999) 32–36.

[20] X. Liu, C. Ding, Plasma sprayed wollastonite/TiO_2 composites coatings on titanium alloys, Biomaterials 23 (2002) 4065–4077.

[21] X. Liu, C. Ding, P.K. Chu, Mechanism of apatite formation on wollastonite coatings in simulated body fluids, Biomaterials 25 (2004) 1755–1761.

[22] X. Liu, C. Ding, Morphology of apatite formed on surface of wollastonite coating soaked in simulated body fluid, Materials Letters 57 (2002) 652–655.

[23] W. Ortega-Lara, D. Cortés-Hernández, S. Best, R. Brooks, L. Bretado-Aragón, D. Rentería-Zamarrón, In vitro bioactivity of wollastonite-titania materials obtained by sol–gel method or solid state reaction, Journal of Sol–Gel Science and Technology 48 (2008) 362–368.

[24] T. Kokubo, H. Kushitani, S. Sakka, T. Kitsugi, T. Yamamuro, Solutions able to reproduce in vivo surface-structure changes in bioactive glass-ceramic A-W, Journal of Biomedical Materials Research 24 (1990) 721–734.

[25] N. Serpone, D. Lawless, R. Khairutdinov, Size effects on the photophysical properties of colloidal anatase TiO_2 particles: size quantization or direct transitions in this indirect semiconductor? Journal of Physical Chemistry 99 (1995) 16646–16654.

[26] W.A. Daoud, J.H. Xing, Y.H. Zhang, Surface functionalization of cellulose fibers with titanium dioxide nanoparticles and their combined bacterial activities, Surface Science 599 (2005) 69–75.

[27] U. Meyer, A. Büchert, H.P. Wiessmann, U. Joos, D.B. Jones, Basic reactions in osteoblast on structured materials surfaces, European Cells and Materials Journal 9 (2005) 39–49.

[28] P. Roach, D. Eglin, K. Rohde, C.C. Perry, Modern biomaterials: a review-bulk properties and implications of surface modifications, Journal of Materials Science: Materials in Medicine 18 (2007) 1263–1277.

[29] B.D. Boyan, C.H. Lohmann, D.D. Dean, V.L. Sylvia, D.L. Cochran, Z. Swuartz, Mechanism involved in osteoblast response to implant surface morphology, Annual Review of Materials Research 31 (2002) 357–371.
[30] M. Bachle, R.J. Kohal, A systematic review of the influence of different titanium surface on proliferation, on differentiation and protein synthesis of osteoblast-like MG63 cells, Clinical Oral Implants Research 15 (2004) 683–692.
[31] H.K Kim, J.W. Jang, C.H. Lee, Surface modification of implant materials and its effect on attachment and proliferation of bone cell, Journal of Materials Science: Materials in Medicine 15 (2004) 825–830.
[32] O. Zinger, K. Anselme, A. Denzer, P. Hatbersetzer, M. Wieland, J. Jeanfilds, P. Hardouin, D. Landonlt, Time-dependent morphology and adhesion of osteoblastic cells on titanium model surfaces featuring scale-resolved topography, Biomaterials 25 (2004) 2695–2711.